Temporal extrapolation of N-uptake maps retrieved from satellite imagery aiming to overcome availability issues due to cloudy days

S. Reusch[1], G. Portz[1]

[1]Research Centre Hanninghof, Yara International ASA, Hanninghof 35, 48249 Duelmen, Germany. (stefan.reusch@yara.com)

A paper from the Proceedings of the

17th International Conference on Precision Agriculture and 11th Brazilian Congress on Precision and Digital Agriculture

13-15 July 2026

Porto Alegre, Brazil

Abstract.

Several satellite-based functionalities, including in-field variable-rate nitrogen fertilization, require an up-to-date satellite image. Under cloudy conditions, current imagery may be compromised or unavailable. To overcome this issue and obtain an image representing current field status, a simple crop growth model was created to temporally extrapolate crop growth from the last available image. The model was implemented in a fully automated processing chain consisting of the following steps: First, the latest cloud-free image for a given field is retrieved, and previously established relationships are applied to compute both above-ground nitrogen uptake and dry matter for each pixel in the image. Then, an irradiance-driven crop growth model is run iteratively to compute daily dry matter increase until the present date or another target date. Required weather parameters, such as daily irradiance, air temperature and air humidity, are retrieved from a global weather service. Finally, the resulting dry matter map is converted to N-uptake and returned either for display or for further processing into a variable-rate application map. To test and validate the approach, more than 1000 pairs of acquired versus extrapolated winter cereal images collected from farmers' fields in Germany and Sweden between 2017 and 2023 were used. Results show that, without extrapolation, N-uptake on a given day was underestimated by more than 10 kg N/ha on average, with high variability among individual cases. With extrapolation, however, N-uptake estimation was nearly unbiased on average, and RMSE was also significantly reduced, demonstrating that the approach is robust and can be implemented digitally at large scale.

Keywords.

Remote sensing, Crop growth modeling, Variable rate nitrogen fertilization, Crop nutrition.

Introduction

Spatially specific in-season assessment of crop nitrogen (N) status is a prerequisite for site-specific N fertilization, because within-field differences in biomass accumulation and N-uptake directly influence yield formation. The in-field variability of those factors can therefore be used to drive the fertilization right dose at the right field spot and right moment in the season, mitigating the risk of inefficient fertilizer use. In winter cereals, optical satellite data with field-scale spatial resolution and red-edge-sensitive information have made operational retrieval of above-ground N-uptake increasingly feasible, assisting decision-support systems for variable-rate N management (Delloye et al. 2018, Bossung et al. 2022, Wolters et al. 2021, Li et al. 2022). However, the principal bottleneck of remote satellite data is temporal rather than purely spatial. Orbital monitoring systems remain dependent on cloud-free acquisitions, and critical fertilizer top-dressing windows may therefore coincide with missing or heavily compromised imagery (Eberhardt et al. 2016, Zhou et al. 2025).

Recent developments to overcome this issue have advanced along three complementary directions. First, several studies have improved the retrieval of N-related variables from available imagery through vegetation indices, empirical and machine-learning models, or radiative-transfer inversion, with useful results for wheat N-uptake at field and sub-field scales (Delloye et al. 2018, Bossung et al. 2022, Wolters et al. 2021, Li et al. 2022). Second, cloud-related discontinuities have been addressed through gap-filling and multi-sensor approaches, including learning-based fusion of optical and radar time series to recover continuous agricultural observations (Zhou et al. 2025, Tsardanidis et al. 2025). Third, remote sensing has increasingly been coupled with crop growth models and decision rules so that temporally sparse observations can inform in-season crop N status rather than only post hoc observation (Huang et al. 2019, Piikki et al. 2022, Gobbo et al. 2022). Taken together, this literature suggests that remote sensing becomes most agronomically valuable when it is embedded in an operational decision framework rather than treated as an isolated mapping exercise.

However, a practical gap remains between remote sensing research and day-to-day applicable field operations. Many published workflows still depend on imagery obtained sufficiently close to the management date, or they reconstruct time series of reflectance indices without directly producing an agronomic variable needed by fertilization workflows, namely an up-to-date map of crop N-uptake or a closely related crop-status indicator (Zhou et al. 2025, Huang et al. 2019, Tsardanidis et al. 2025). Furthermore, more advanced fusion and assimilation strategies can also introduce additional data requirements, calibration effort and computational demands, which can limit their scalability across different fields, regions and growing seasons.

To address these constraints, this paper presents a deliberately operational alternative: it starts from the latest cloud-free satellite image, derives pixel-level dry matter and N-uptake, temporally extrapolates crop growth to the target date using an irradiance-driven crop growth model and routine weather data, and returns an updated N-uptake map for visualization or variable-rate application. Focusing on temporal extrapolation of agronomically interpretable maps, the paper addresses a concrete obstacle to satellite-enabled precision fertilization under cloudy conditions.

Material and methods

Satellite images

The data processing chain starts with the retrieval of the latest cloud-free satellite image (ESA Sentinel-2) for a given field. For this purpose, the Sentinel Hub API (Sinergise Solutions d.o.o, Ljubljana, Slovenia) is called iteratively to retrieve Level-2A images for the given geometry, starting at the target date (typically the current date) and moving backwards in time until a cloud-free image is found. An image is regarded as cloud-free if, in the scene classification layer (SCL), at least 95% of the pixels within the field boundary are identified as either “dark area” (SCL = 2), “vegetation” (SCL = 4) or “not vegetated” (SCL = 5). This criterion is considered a good compromise for rejecting images that are cloudy or unusable for other reasons while retaining images with only minor distortions. However, since the scene classification is not perfect, a few obviously cloudy or hazy images may still pass, or clear images may be rejected.

N-uptake estimation

Once a cloud-free image is retrieved, the Sentinel-2 bands *B06* (red edge) and *B07* (near-infrared) are extracted and a spectral vegetation index

$$VI = B07 / B06 \tag{1}$$

is calculated for every pixel within the field boundary. This index has been found to correlate well with the above-ground nitrogen uptake (N-uptake) of many crops during the vegetative growth phase. Explicit correlation equations have previously been established in multiple field trials by collecting reflectance spectra using a handheld spectrometer, simulating the abovementioned Sentinel-2 bands from the spectra and relating the calculated *VI* index to N-uptake estimated from subsequent crop sampling and laboratory analysis. Figure 1 shows an example of such a correlation for winter wheat throughout the vegetative growth stages (BBCH 30-59).

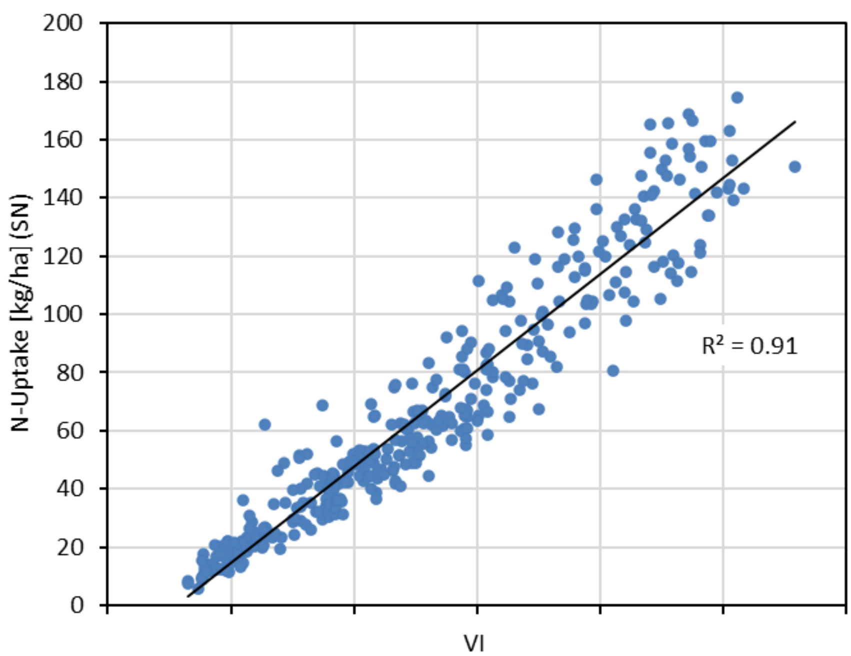

Figure 1: Relationship between vegetation index VI (as simulated from handheld spectrometer) and N-uptake for winter wheat BBCH 30-59 (example)

By applying this (crop-specific) correlation equation g, the *VI* image is converted into an image that contains the N-uptake SN_0 at the date of image acquisition, i. e.:

$$SN_0 = g(VI) \tag{2}$$

Conversion to dry matter

Since the crop model runs on the crop’s above-ground dry matter, the N-uptake is converted to dry matter using the critical nitrogen dilution concept. According to this concept, the nitrogen concentration N_c in a non-nutrient-deficient crop canopy follows a crop-specific dilution curve when the crop biomass *DM* develops:

$N_c = a * DM^{-b}$ for $DM > c$, otherwise $N_c = a$ (3)

where a, b and c are crop-specific parameters. Since the N-uptake is equivalent to the nitrogen concentration N_c times the dry matter DM, this formula can be rewritten to

$SN = \mathrm{f}(DM) = a * DM^{1-b}$ for $DM > c$, otherwise $SN = a * DM * c^{-b}$ (4)

The dry matter at the date of image acquisition is finally calculated by inverting this formula:

$DM_0 = \mathrm{f}^{-1}(SN_0)$ (5)

Crop growth model

A simple irradiance-driven crop growth model is used to iteratively calculate biomass growth in daily time steps from the date of the last available image to the target date. The model uses daily weather data (irradiance, temperature and vapor pressure deficit) supplied by a global historical weather data provider (The Weather Company, Brookhaven, USA) for the geographical location of the field.

The dry matter DM_i for day i+1 after the date of the last image is calculated as

$DM_{i+1} = DM_i + \varepsilon * 0.45 * f_{APAR} * f_T * f_{VPD} * E_i$ (6)

where

ε = 0.042 t MJ^{-1}: radiation use efficiency

f_{APAR}: fraction of absorbed photosynthetic radiation at day i

f_T: temperature efficiency factor at day i

f_{VPD}: humidity efficiency factor at day i

E_i: daily global horizontal irradiance at day i

As the fraction of absorbed photosynthetic radiation f_{APAR} is strongly correlated with light absorbance in the red-edge region of the spectrum (Dong et al. 2015, Kamenova and Dimitrov 2021), f_{APAR} is estimated from the spectral index VI_i at day i using an empirical function. The efficiency factors f_T and f_{VPD} range from 0 (=no growth possible) to 1 (= optimal growth conditions) and are functions of temperature and vapor pressure deficit at day i, respectively (Kemanian et al. 2004).

After each iteration, the resulting dry matter DM_{i+1} is converted back into N-uptake SN_{i+1} using equation (4) and further to VI_{i+1} using the inverse of equation (2). When the target date is reached after t iterations, the processing is stopped and the resulting N-uptake SN_t is returned.

It should be emphasized that the model implicitly assumes non-limiting growing conditions, i. e. severe drought stress, nutrient deficiency or infestation are not considered directly. They may affect the estimated dry matter assimilation only indirectly and with a time delay through a reduction in f_{APAR}. Therefore, particularly short-term crop stress may lead to an overestimation of the N-uptake.

Implementation

The above-mentioned calculations and the model are run for every individual pixel of the image, resulting in a map of estimated N-uptake at the target date.

Figure 2 visualizes the processing steps: satellite images are available every 2nd or 3rd day (bottom row), but, viewed from the target date ("today", May 20th in this example), the latest cloud-free image occurred on May 9th. This image is converted to nitrogen uptake, and the model is then run iteratively in daily time steps until the target date (here: May 20th) is reached.

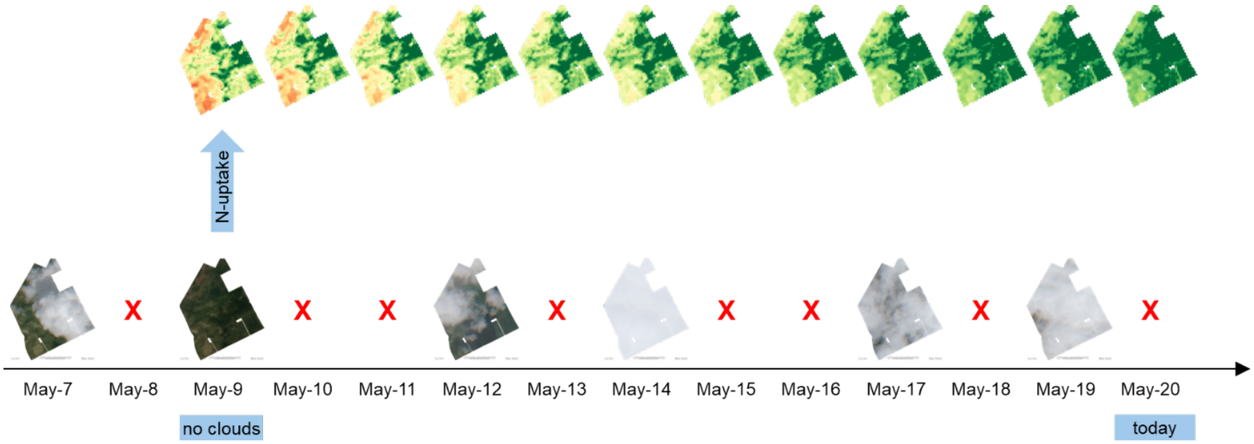

Figure 2: Visualization of the processing steps. The lower row shows the available satellite images, whereas the upper row displays the extrapolated N-uptake maps for every day.

Because the weather data are the same for the whole field and since no further spatial information is used, the extrapolation does not change the spatial pattern of the original N-uptake map. However, since the algorithm is intended to only run for maximum 3-4 weeks, the assumption of stable spatial patterns seems reasonable for this limited time period.

Example

Figure 3 shows N-uptake maps generated for a winter wheat field in central Germany (52.782°N, 11.530°E). The left map was generated from a cloud-free satellite image acquired on April 11th, 2022 using equation (2). The average N-uptake is 27 kg N/ha. The map in the middle shows the result of the extrapolation to the target date, April 29th, 2022 (i. e. 18 days). According to the extrapolation algorithm, field-average N-uptake has increased by 39 kg N/ha to 66 kg N/ha. In comparison, the average N-uptake estimated from a cloud-free image on the same day is 68 kg N/ha and the spatial patterns in the field are very similar (right map).

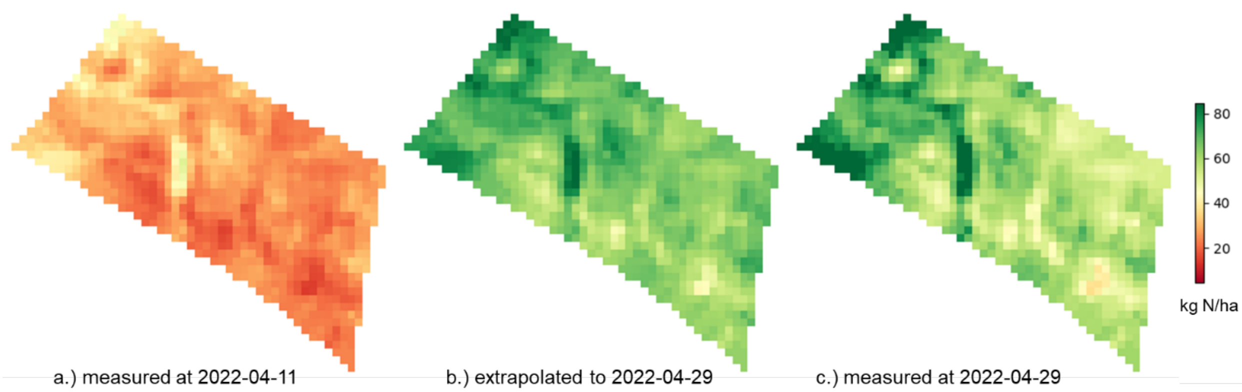

Figure 3: N-uptake in a winter wheat field in Germany: a.) estimated from a cloud-free satellite image on Apr 11th, b.) extrapolated from Apr 11th to Apr 29th and c.) from a cloud-free satellite image on Apr 29th

Figure 4 displays the average N-uptake for the vegetative part of the growing season (from March 1st to June 15th) as extrapolated using the crop growth model. Model runs start on each date with a cloud-free image (blue crosses) and stop when the next cloud-free image becomes available. At that date the modelled N-uptake can be compared with the N-uptake as directly estimated from the image. In this example, very good matches are found for the model runs ending on April 9th, April 29th and May 9th. On May 16th and on June 3rd the model overestimates the N-uptake by 17 kg N/ha and by 25 kg N/ha, respectively.

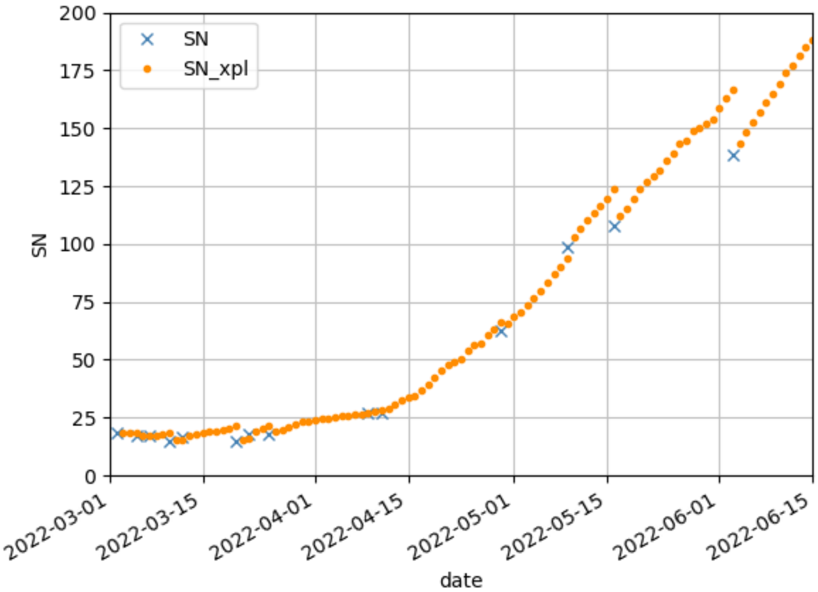

Figure 4: Field-average N-uptake for the field in Figure 3Figure 2 as estimated from cloud-free satellite images (blue crosses) and from the extrapolation algorithm (orange dots). Extrapolation starts every time a new cloud-free image becomes available and runs until the next cloud-free image.

Accuracy estimation

Dataset

Satellite data were retrieved from farmers' fields located at 7 farms in Germany and 3 farms in Sweden. Only fields and seasons with winter cereals (winter wheat, winter barley or winter rye) grown between 2017 and 2023 were selected, resulting in a total of 182 site-years (see Table 1).

Farm	No. of fields in year…							
	2017	2018	2019	2020	2021	2022	2023	*Total*
Eistrup (DE)			1	1	2	1	1	*6*
Federolf (DE)			1	2	3	1	2	*9*
Große-Scharmann (DE)	5	5	8	9	6	2		*35*
Lückstedt (DE)						25	5	*30*
Rittergut-Vahlberg (DE)		1	1	1				*3*
Sprenker (DE)			1	2	3	5	1	*12*
Ziesetal (DE)	1	3	5	5	2			*16*
Bjertorp (SE)	7	3	12	12	14			*48*
Kärret (SE)	4		4					*8*
Kyrkobacka (SE)	3	3	2	3	4			*15*

Table 1: No. of fields in the dataset per farm and year

For each site-year, all available cloud-free Sentinel-2 level 2A images were retrieved for the period in which the growing degree days (defined as the sum of daily mean temperature above 0°C starting on March 1st) ranged between 100°C and 700°C. In this dataset, this period typically comprises the months of April and May and is regarded as most relevant for N-uptake monitoring.

Overall, this resulted in 1398 pairs of consecutive cloud-free images with time gaps of 1 to 28 days between individual acquisitions. In other words, each image pair consists of a "start" image, an "end" image and the number of days in-between them.

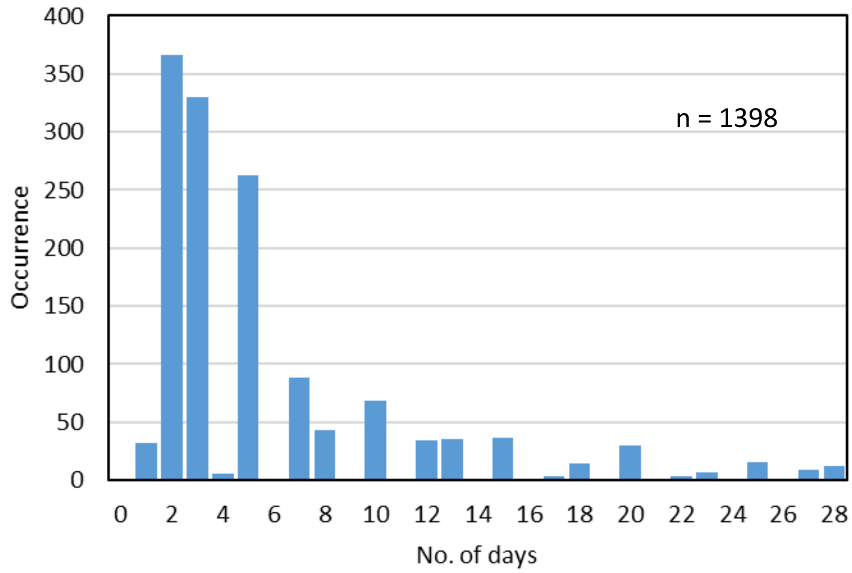

Figure 5: Number of days between two consecutive cloud-free images in the dataset

Figure 2Figure 5 shows the distribution of the number of days (gap) between the two images in each pair across the whole dataset. Most gaps are 2, 3 or 5 days, reflecting the revisit time of Sentinel-2 at higher latitudes. However, there are also several cases in which cloudy periods resulted in image gaps of 10 days or more. The longest gap found in this dataset was 28 days.

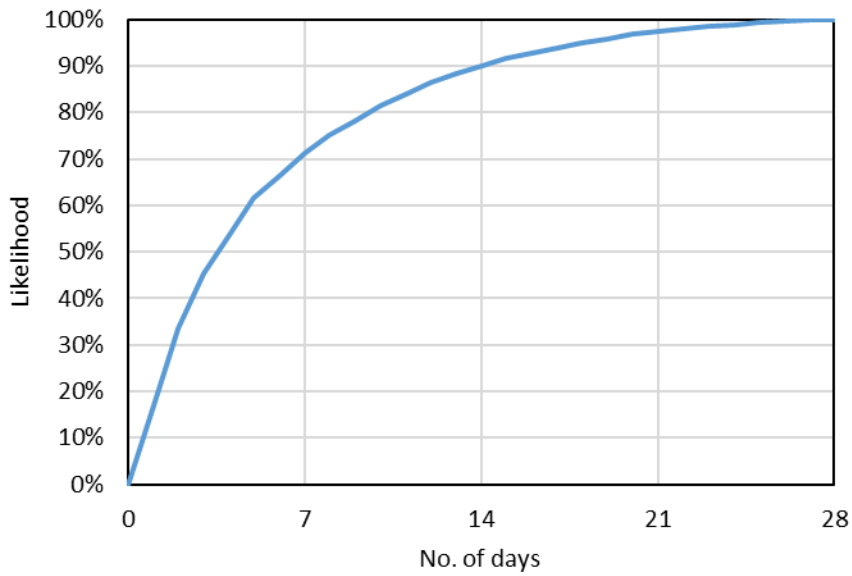

Figure 6: Likelihood of getting a cloud-free image within a given time period

Figure 6 shows the more relevant likelihood of obtaining a cloud-free image within a given number of days. As can be seen, the likelihood of obtaining an image within 7 days is 70%. A maximum image age of 14 days can be expected with a likelihood of 90%, and, if a 3-week-old image is acceptable, this could have been provided with a likelihood of 97%.

Errors without and with extrapolation

To quantify the potential error in N-uptake estimation when an outdated image is used, for each of the 1398 consecutive image pairs the field-average N-uptake was computed using equation (2) for both the “start” and the “end” image, respectively. Without extrapolation and without having the “end” image available, the best guess for the N-uptake at the date of the “end” image would be the unaltered N-uptake from the “start” image. This unaltered N-uptake is compared to the “real” N-uptake retrieved from the “end” image and the difference *ΔN-uptake* is computed. Figure 7 (left) shows the distribution of these differences across the whole dataset as well as the respective statistics.

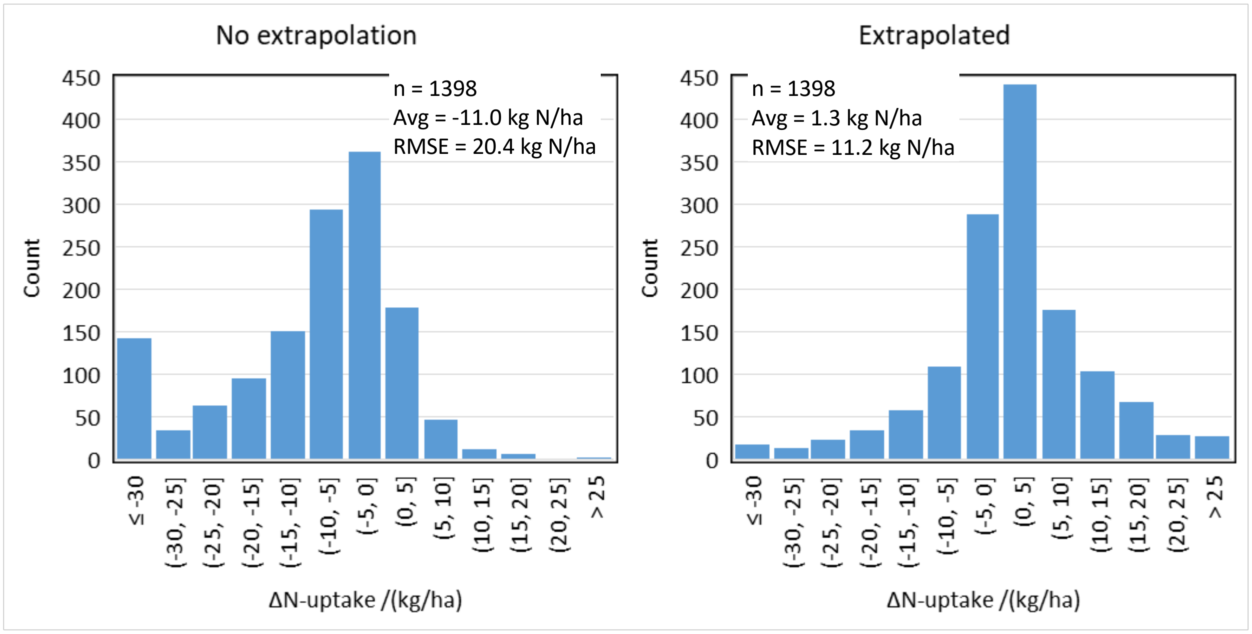

Figure 7: Distribution of N-uptake estimation errors across the dataset, using the last available image as-is (left) and extrapolating this image to the current date (right).

As expected, determining N-uptake from the last available image alone leads to an average underestimation of 11.0 kg N/ha on the day when, or just before, the next image becomes available. In addition, the variability of the error is large (RMSE = 20.4 kg N/ha). In about 10% of cases, N-uptake would be underestimated by 30 kg N/ha or more.

In contrast, when running the extrapolation from the “start” image to the “end” date the average difference between the extrapolated N-uptake and the N-uptake estimated from the “end” image is negligible (1.3 kg N/ha overestimation) and the variability is much lower (RMSE = 11.2 kg N/ha), see Figure 7 (right). The number of extreme cases with absolute errors |*ΔN-uptake*| ≥ 30 kg N/ha is reduced to about 1%.

To quantify the effect of image latency on the accuracy of N-uptake estimation, the dataset was grouped into classes according to the number of weeks after the last available image, and the average and standard deviation of *ΔN-uptake* were calculated per group (Figure 8).

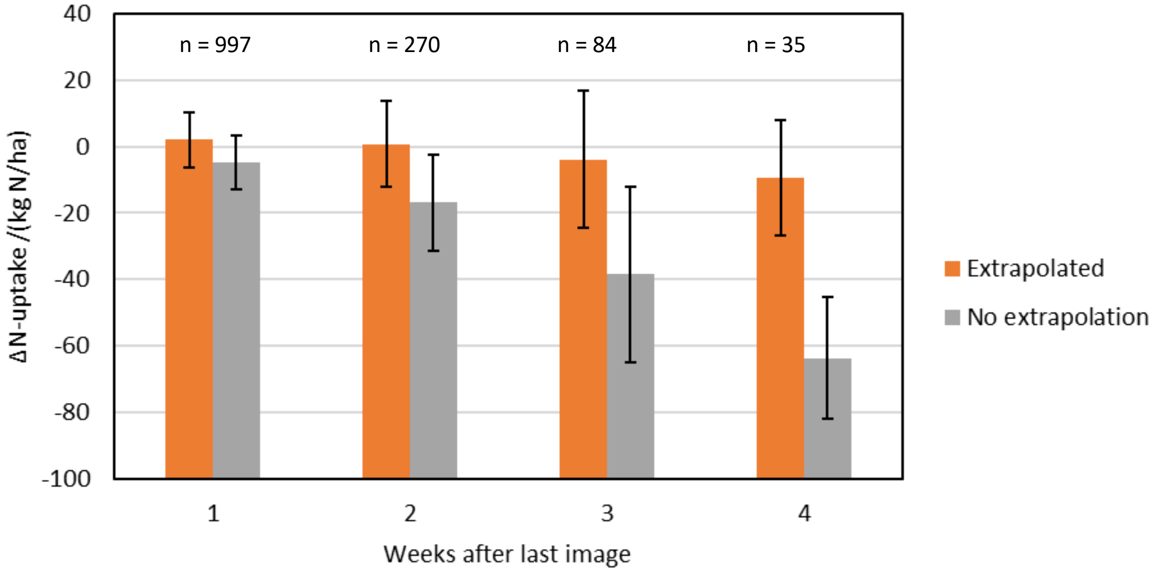

Figure 8: Average error of N-uptake estimation with (orange) and without (grey) extrapolation as a function of the number of weeks after the last cloud-free image. The error bars indicate ±1 standard deviation.

As shown, without extrapolation the N-uptake is underestimated by about 20, 40 and 60 kg N/ha after 2, 3 and 4 weeks without any new image, respectively. With extrapolation, however, the average error can be kept below 5 kg N/ha for the first 3 weeks and increases to only 10 kg N/ha in week 4.

Since – at least in this dataset – the maximum time gap between two cloud-free images is 28 days, it can be concluded that image extrapolation can effectively bridge all cloudy periods observed in this dataset. In individual cases, errors may be up to 30 kg N/ha, but on average the deviation is below 10 kg N/ha. Therefore, this approach is suitable for practically and in a scalable way overcoming the problem of limited image availability, which is often referred to in the context of time-sensitive nitrogen management.

Summary

Timely availability of cloud-free satellite imagery remains a major limitation for operational, satellite-based variable-rate nitrogen fertilization. This paper presents and evaluates an automated workflow that uses the latest available cloud-free Sentinel-2 image as a starting point, converts spectral information into pixel-level N-uptake, and extrapolates crop development to a target date with a simple irradiance-driven growth model using globally available routine weather data.

Evaluation was carried out on farmers' fields of winter cereals in Germany and Sweden from 2017 to 2023. Results indicate that temporal extrapolation can effectively bridge typical cloud-induced gaps in satellite image availability during the relevant spring fertilization period. For image gaps of up to three weeks, the average error remained below 5 kg N/ha, and even in the fourth week the mean deviation was only about 10 kg N/ha. The method therefore provides a practical and scalable means of generating up-to-date N-uptake maps for visualization and downstream generation of variable-rate application maps. Its simplicity is also its main limitation: the model assumes non-limiting growth conditions and does not explicitly account for severe drought, nutrient deficiency, pest damage, or other stress factors. Future work should therefore focus on integrating stress indicators and additional data sources while preserving the robustness and automation required for large-scale operational use.

References

Bossung, C., Schlerf, M., Machwitz, M. (2022) Estimation of canopy nitrogen content in winter wheat from Sentinel-2 images for operational agricultural monitoring, *Precision Agriculture*, 23, 2229–2252. https://doi.org/10.1007/s11119-022-09918-y

Delloye, C., Weiss, M., and Defourny, P. (2018). Retrieval of the canopy chlorophyll content from Sentinel-2 spectral bands to estimate nitrogen uptake in intensive winter wheat cropping systems, *Remote Sensing of Environment*, 216, 245–261. https://doi.org/10.1016/j.rse.2018.06.037

Dong, T., Meng, J., Shang, J., Liu, J., & Wu, B. (2015). Evaluation of chlorophyll-related vegetation indices using simulated Sentinel-2 data for estimation of crop fraction of absorbed photosynthetically active radiation." *IEEE Journal of Selected Topics in Applied Earth Observations and Remote Sensing*, 8(8), 4049–4059. https://doi.org/10.1109/jstars.2015.2400134

Eberhardt, I. D. R., Schultz, B., Rizzi, R., Sanches, I. D., Formaggio, A. R., Atzberger, C., Mello, M. P., Immitzer, M., Trabaquini, K., Foschiera, W., Luiz, A. J. B. (2016). Cloud Cover Assessment for Operational Crop Monitoring Systems in Tropical Areas, *Remote Sensing*, 8(3), 216. https://doi.org/10.3390/rs8030219

Gobbo, S., De Antoni Migliorati, M., Ferrise, R., Morari, F., Furlan, L., Sartori, L. (2022). Evaluation of different crop model-based approaches for variable rate nitrogen fertilization in winter wheat, *Precision Agriculture*, 23, 1922–1948. https://doi.org/10.1007/s11119-022-09957-5

Huang, J., Gómez-Dans, J. L., Huang, H., Ma, H., Wu, Q., Lewis, P. E., Liang, S., Chen, Z., Xue, J.-H., Wu, Y., Zhao, F., Wang, J., Xie, X. (2019). Assimilation of remote sensing into crop growth models: Current status and perspectives, *Agricultural and Forest Meteorology*, 276, 107609. https://doi.org/10.1016/j.agrformet.2019.06.008

Kamenova, I., Dimitrov, P. (2021). Evaluation of Sentinel-2 vegetation indices for prediction of LAI, fAPAR and fCover of winter wheat in Bulgaria, *European Journal of Remote Sensing*, 54, 89-108. https://doi.org/10.1080/22797254.2020.1839359

Kemanian, A. R., Stöckle, C. O., Huggins, D. R. (2004). Variability of barley radiation use efficiency. *Crop Science*, 44, 1662-1672. https://doi.org/10.2135/cropsci2004.1662

Li, X., Ata-Ul-Karim, S. T., Li, Y., Yuan, F., Miao, Y., Kato, Y., Cheng, T., Tang, L., Tian, X., Liu, X., Tian, Y., Zhu, Y., Cao, W., Cao, Q. (2022). Advances in the estimations and applications of critical nitrogen dilution curve and nitrogen nutrition index of major cereal crops. A review, *Computers and Electronics in Agriculture*, 197, 106998. https://doi.org/10.1016/j.compag.2022.106998

Piikki, K., Söderström, M., Stadig, H. (2022). Remote sensing and on-farm experiments for determining in-season nitrogen rates in winter wheat – Options for implementation, model accuracy and remaining challenges, *Field Crops Research*, 289, https://doi.org/10.1016/j.fcr.2022.108742

Tsardanidis, I., Koukos, A., Sitokonstantinou, V., Drivas, T., Kontoes, C. (2025). Cloud gap-filling with deep learning for improved grassland monitoring, *Computers and Electronics in Agriculture*, 230, 109732. https://doi.org/10.1016/j.compag.2024.109732

Wolters, S., Söderström, M., Piikki, K., Reese, H., Stenberg, M. (2021). Upscaling proximal sensor N-uptake predictions in winter wheat (Triticum aestivum L.) with Sentinel-2 satellite data for use in a decision support system, *Precision Agriculture*, 22, 1263–1283. https://doi.org/10.1007/s11119-020-09783-7

Zhou, Y., Ma, Y., Ata-Ul-Karim, S. T., Wang, S., Ciampitti, I., Antoniuk, V., Wu, C., Andersen, M. N., Cammarano, D. (2025). Integrating multi-angle and multi-scale remote sensing for precision nitrogen management in agriculture: A review, *Computers and Electronics in Agriculture*, 230, 109829. https://doi.org/10.1016/j.compag.2024.109829